Mathematical Biosciences and Engineering, 16(4): 2371–2390.
DOI: 10.3934/mbe.2019119
Received: 13 January 2019
Accepted: 28 February 2019
Published: 15 March 2019

http://www.aimspress.com/journal/MBE

Research article

Performance of cement-stabilized macadam roads based on aggregate gradation interpolation tests

Zhijun Liu*, Xiaobi Wei, Dongquan Wang and Liangliang Wang

State Key Laboratory for Geomechanics and Deep Underground Engineering, School of Mechanics & Civil Engineering, China University of Mining & Technology, Xuzhou 221116, China

*** Correspondence:** Email: zhijunlcn@yeah.net; Tel: +8613852107266.

Abstract: This study adopted the uniform interpolation method to obtain five gradation types (labeled A, B, C, D, and E, from "coarse-grained" to "fine-grained" types) based on the skeleton dense structure and cement-stabilized macadam (CSM) aggregate gradation range recommended by current specifications. The optimum water content of the CSM exhibited a linear increase with gradation, whereas the maximum dry density exhibited a variation that can be described by a quadratic curve, for which the peak maximum dry density was near the maximum dry density of the Type B gradation. In the CSM structure, the skeleton void effect of the coarse-grained aggregate, the filling effect of the fine-grained aggregate, and the cementation effect of the cement and aggregate exhibited corresponding fluctuations. The ability to resist temperature shrinkage deformation was reduced. Additionally, the optimum values of the compressive strength and compression rebound modulus of the CSM plotted near the curve of the Type D gradation.

Keywords: CSM; aggregate gradation; skeleton dense structure; uniform interpolation; road performance; experimental study

1. Introduction

As a major semirigid base course material, cement-stabilized macadam (CSM) is widely applied in pavement engineering, and its quality has considerably influenced the quality of the resulting road structures. Therefore, research on the road performance of CSM has been of considerable interest [1–5].

Numerous studies have shown that the engineering performance of the cement base material,

such as its strength, rigidity and shrinkage, is mainly influenced by specific material characteristics [6–10]. Aggregate is the main raw material and has a noticeable influence on the performance of cement-based material. Although structural concrete and mortar are widely applied in engineering construction, high-quality aggregate is required. In projects with demolition, superplasticizer can greatly enhance the performance of mortars produced with construction and demolition waste aggregate; in particular, the aggregate obtained from bricks can greatly improve the mechanical strength of the composite [11]. In a study on the use of polyolefin waste aggregate (PWA) obtained from recycled plastic material as the substitute for natural aggregate in the production of lightweight aggregate concrete (LWAC), Colangelo et al. found that the performance of the concrete worsened with the increase in the substitute material when different amounts of the natural aggregate were replaced by the same amount of PWA; in addition, as the percentage of the recycled aggregate increased, the compressive strength of the product was reduced when exposed to elevated temperature up to 600 ℃ [12].

CSM is a cement-based material. Although the type and fineness of the aggregate have a great influence on the performance of CSM, the aggregate grade has received more attention than its other properties, which can also significantly influence the road performance of CSM [2,13]. The compressive strength and workability of the concrete can be greatly influenced by aggregate gradation, and by changing aggregate gradation, the compressive strength of the concrete can be increased by approximately 50% [14]. Fatmi et al. reported that the strengths of concrete prepared with different mix design ratios and a combined gradation of prepared single-sized aggregates were approximately 20% higher than those of concrete prepared with the same design mix and combinations of aggregate gradation [15]. Jin and Zheng selected CSMs of five gradations for compressive strength tests and comparisons, which they used to determine the optimum gradation type [16]. The selection of an aggregate gradation is important for the design of concrete mixtures; although some aggregate gradations can greatly improve the performance of concrete mixtures, others may result in poor outcomes [17]. According to the aggregate gradation method, the Ministry of Communications of PRC also classifies CSM into three categories, namely, those with a skeleton dense structure (the void volume of the coarse aggregate is similar to the volume of the fine aggregate after compaction), skeleton void structure (the void volume of the coarse aggregate is larger than the volume of the fine aggregate after compaction) and skeleton suspension structure (the void volume of the coarse aggregate is smaller than the volume of the fine aggregate after compaction), based on the upper and lower limits of the sieve-passing rate for each aggregate particle size [18]. Hu studied the strength properties and modulus characteristics through laboratory experiments and found that different types of cement gravel structures had different properties and that frame cement-stabilized aggregates exhibited excellent road performance [19]. Liu and Li studied the unconfined compressive strength, splitting strength, and dry shrinkage of CSM specimens with 16 aggregate grades using the orthogonal experimental design method and found that the contents of coarse aggregate with a particle size larger than 13.2 mm and fine aggregate with a particle size of 2.36 mm are directly related to the formation of the skeleton dense structure and are the most influential factors [20]. Scholars have conducted indoor performance tests considering different gradation types and different CSM mixtures to study the mechanical performance and shrinkage performance of each mixture [5,21–23]. The results indicated that the unconfined compressive strength and splitting strength of the midrange grade mixtures were the best, whereas the dry shrinkage performance was the best for mixtures that included fine gradations.

Coarse-grained mixes with high contents of fine grains exhibited better dry shrinkage performance; however, the temperature shrinkage performance of these types of materials was worse than that of open-grained mixes. Jiang, et al. performed tests on CSM of different gradation types and concluded that CSM with a skeleton dense structure showed better crack resistance than those with skeleton void or suspension structures [24].

Generally, previous studies have obtained useful results for various applications of CSM. However, few studies have provided specific quantitative descriptions of the effect of gradation on the CSM performance index variations and the associated mechanisms. Currently, CSM applications in actual engineering typically employ skeleton dense structures, and the aggregate gradation design of the material is generally based on the median of the recommended range (that is, following the gradation median curve). However, in the construction control process, the actual gradation constructed generally deviates from the designed median curve, and the strength and modulus and other road performance indexes of the CSM material mixed in this manner deviate from the initially designed values due to differences in many factors, including the aggregate source and mixing machinery. Many engineering units are unable to reasonably quantify these deviations due to a lack of equipment with which to perform actual measurements.

Based on the aforementioned issues, this study adopted the uniform interpolation method in the aggregate gradation range to regularly obtain different gradations based on the skeleton dense structure gradation recommended by the current specifications. We studied the effects of the influential patterns and acting mechanisms of the aggregate gradations on the CSM road performance via indoor experimental tests and obtained qualitative relationships between the CSM gradations and geotechnical physical parameters, mechanical parameters, and shrinkage performance indexes to facilitate assessments of CSM performance parameters based on the gradation type, thereby providing a foundation for the application of CSM materials in engineering.

2. Materials and methods

2.1. Materials

The cement used in the experimentation was a commonly used silicate cement (Hanbang "P·O42.5"; Huaihai Cement Plant, Xuzhou, China). The main technical parameters are provided in Table 1. The aggregate, produced in the Xuzhou area, was primarily composed of calcite, accompanied by dolomite, magnesite and limestone, as well as a small proportion of impurities. The material possesses excellent processability, polishability, and cementation, with a crushing value of 20.7% (according to the Ministry of Communications of PRC [25], the aggregate crushing value should not exceed 22%).

Table 1. Comparisons of the technical parameters of the cement used in this study and the standards.

Index	Category	
	Standard	Cement in this study
Loss on ignition (%)	<5	4.7
Fineness sieving allowance (%) (80 μm square hole sieve)	<10	9.1
Setting time (min)		
Initial setting time	≥45	85
Final setting time	≤600	520
Unconfined compressive strength (MPa)		
3 d	≥16	20.5
28 d	≥32.5	35.3
Rupture strength (MPa)		
3 d	≥3.5	3.9
28 d	≥6.5	7.1

2.2. Mixture proportion design

The CSM mixture proportion design includes the determination of the respective proportions of the basic raw materials (cement and macadam aggregate). It also includes the determination of the gradation of the aggregate.

In this experiment, the cement content of the CSM was 4.0%, as is commonly used in engineering practice [26,27], and the aggregate content was 96%, with a mass ratio of 4:96.

To better determine regularity and provide better theoretical support for engineering applications, this study adopted the uniform interpolation method, i.e., 25%, 50%, and 75% intervals between the upper- and lower-limit values of the passing rate at each particle size [18], to obtain three intermediate gradation curves. The equation for interpolation is as follows:

$$Y_{ij}=X_{ij}\cdot(E_j-A_j)+A_j \tag{1}$$

where i is the gradation type, including types B, C, and D; j is the mesh aperture (mm); Y_{ij} is the sieve-passing rate of the aggregate corresponding to the aperture j of the ith gradation type; X_{ij} is the interpolation coefficient, where X_{Bj} = 1/4, X_{Cj} = 1/2, and X_{Dj} = 3/4; and E_j and A_j are the passing rates for aperture j corresponding to types A and E, respectively.

The three interpolation curves, as well as the upper- and lower-limit curves, present five gradations, denoted as A–E from bottom to top, as shown in Figure 1. The results of the aggregate particle sieving are provided in Table 2.

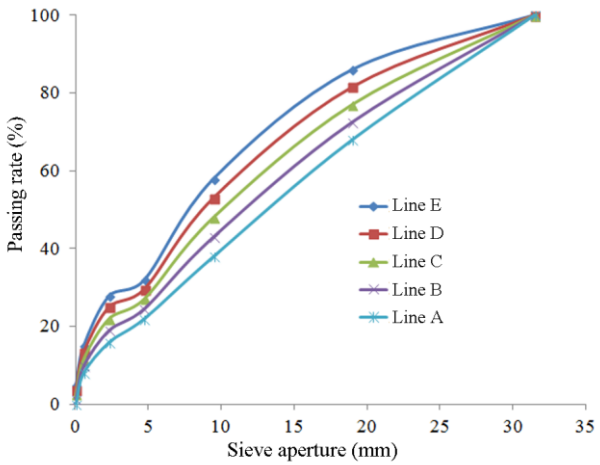

Figure 1. Uniform interpolation curve of aggregate gradation.

Table 2. Aggregate gradation.

Size of square mesh sieve (mm)	Passing rate of various gradations (%)				
	A	B	C	D	E
31.5	100.0	100.0	100.0	100.0	100.0
19	68.0	72.5	77.0	81.5	86.0
9.5	38.0	43.0	48.0	53.0	58.0
4.75	22.0	24.5	27.0	29.5	32.0
2.36	16.0	19.0	22.0	25.0	28.0
0.6	8.0	9.8	11.5	13.3	15.0
0.075	0.0	1.3	2.5	3.8	5.0

2.3. Test design

This experiment mainly tested the geotechnical physical parameters (maximum dry density and optimum water content), mechanical parameters (unconfined compressive strength, splitting strength, and compression rebound modulus) [25], and shrinkage performance parameters (dry shrinkage coefficient and temperature shrinkage coefficient) of the CSM mixtures prepared according to the above five gradation curves.

2.3.1. Optimum water content and maximum dry density

The optimum water content and maximum dry density were determined with reference to the compaction test proposed by the Ministry of Communications of PRC [25]. Under a fixed cement content of 4.0%, the CSM mixtures prepared with different gradations were analyzed via compaction tests. According to practical experience, water contents of 3%, 4%, 5%, 6%, 7%, and 8% were adopted. Specimens were formed using the 3-layer compaction method [25]. Specifically, the material was hammered 94 times after each layer was loaded. After hammering, the surface was leveled, and another layer of material was loaded. After the specimens were compacted, the water content and dry density were measured and then plotted in the corresponding coordinate system.

Then, quadratic curve fitting was performed to derive the optimum water content and maximum dry density [25].

2.3.2. Mechanical parameters

The specimens analyzed in the mechanical property test were normally cylindrical specimens with a diameter of 150 mm and a height of 150 mm [25]. The unconfined compressive strength, splitting strength, and compression rebound modulus of the mixture were tested for each type of gradation curve.

Specimens were made in accordance with the standard stipulated by the Ministry of Communications of PRC (T0843-2009) (Figure 2) [25]. The cement and the aggregate were added into a basin according to a mass ratio of 4:96.

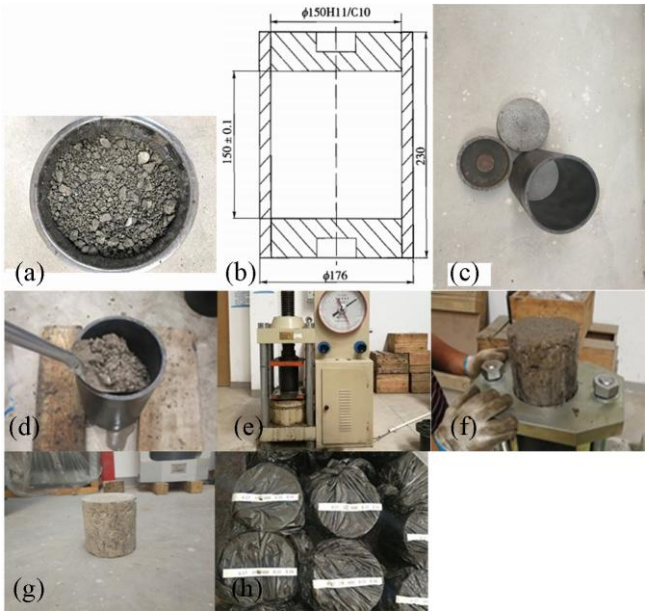

Figure 2. Procedures of specimen fabrication for the mechanical performance tests: a: material mixing; b: sizes of the mold and the block (unit, mm); c: mold and block equipment; d: material loading; e: static pressing; f: demolding; g: formed specimen; h: specimen curing.

After the specimens were molded, the specimens used for the unconfined compressive strength test were cured for 7 days, whereas the specimens used to test the splitting strength and compression rebound modulus were cured for 90 days.

The unconfined compressive strength test and the splitting strength test were performed in accordance with the standards stipulated by the Ministry of Communications of PRC (Items T0805-1994 and T0806-1994, respectively) [25]. Briefly, a press with an appropriate measuring range was selected (the specimen failure load should be within 20–80% of the range), and the loading rate was controlled to be 1 mm/min. The specimen was submerged in water for 1 day before the experiment. The specimen was applied onto the press, and the maximum pressure P (N) was recorded at the time that failure occurred. For the parallel specimens in the same group, outliers were

removed using the three times mean square deviation method: Only 2–3 outliers were allowed; otherwise, the experiment should be reperformed. The coefficient of variation among specimens in the same group should be ≤15%. Otherwise, more specimens should be added.

The compression rebound modulus test was performed in accordance with Item T0808-1994 from the Ministry of Communications of PRC [25]. A displacement transducer-attached press with an appropriate measuring range was selected. The loading rate was controlled to be 1 mm/min. The actual loaded maximum unit pressure was slightly greater than the selected value on the loading plate (0.5–0.7 MPa). The specimen was submerged in water for 1 d before the test. Precompression was performed, during which half of the maximum load to be applied was loaded and unloaded (twice). The preset unit pressure was divided into five equal levels, which were used as the pressure values for each loading time. The first level of pressure was applied and stabilized for 1 min, and then unloading was performed to allow the specimen to rebound from elastic deformation. After 0.5 min, the next level of pressure was applied. The transducer calculated the first rebound deformation under each load level based on the displacement data. A p-1 curve was plotted, and the false deformation was corrected. For parallel specimens in the same group, outliers were removed using the three times mean square deviation method. The coefficient of variation among specimens in the same group was ≤15%.

The mechanical property tests are shown in Figure 3.

Figure 3. Mechanical property tests: a: unconfined compressive strength test; b: splitting strength test; c: compression rebound modulus test.

The mechanical parameters were calculated according to Eqs 2–4 [25].

$$R_c=0.00005659\times10^{-5}\bullet P \tag{2}$$

$$R_i=0.004178\times10^{-3}\bullet P/h \tag{3}$$

$$E_c=p\bullet h/l \tag{4}$$

where R_c is the unconfined compressive strength (MPa) of the specimen, R_i is the splitting strength (MPa), P is the maximum pressure (N) when the specimen breaks, h is the height (mm) of the specimen when it is fully saturated with water, E_c is the compression rebound modulus (MPa), p is the unit pressure (MPa), and l is the rebound deformation.

2.3.3. Shrinkage performance parameters

According to the CSM shrinkage test method [25], beam specimens with dimensions of 400 × 100 × 100 mm^3 (length, width, and height, respectively) were adopted for the test. The dry shrinkage coefficient and temperature shrinkage coefficient were determined for the shrinkage test. Six parallel specimens were used in the dry shrinkage test, whereas three parallel specimens were used for the temperature shrinkage test. The test specimens were molded via the static pressure method (Figure 4) [25], with a compaction degree of 98%.

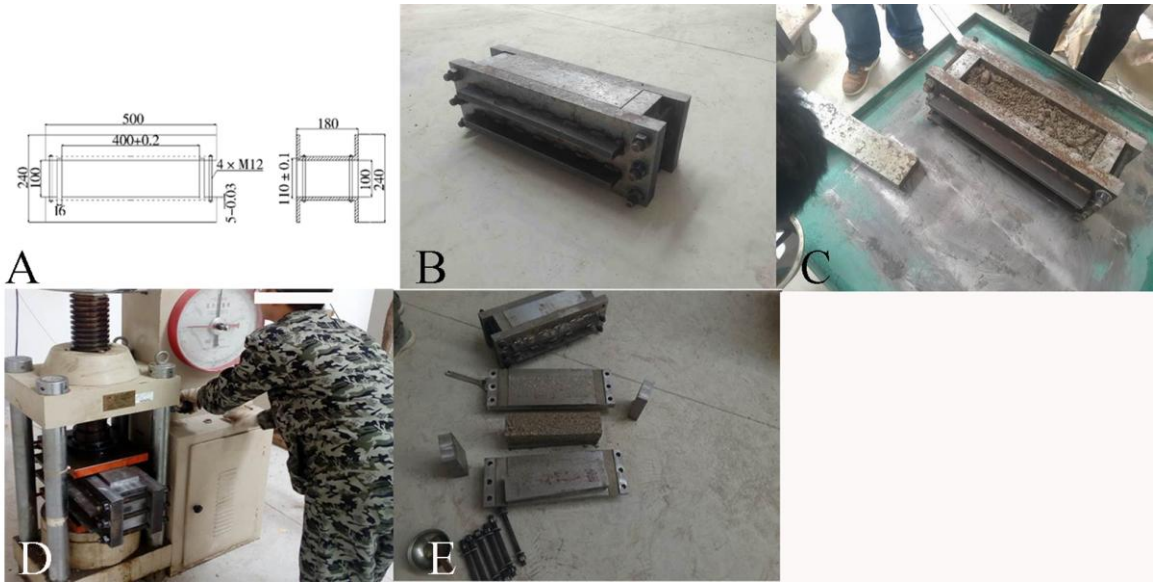

Figure 4. Specimen fabrication for the shrinkage performance tests: a: size of the mold; b: real object of the mold; c: material loading; d: compaction; E: demolding.

After the specimens were molded, they were placed in a room with a constant temperature of (20 ± 2) ℃ for 7 days of curing. Then, the dry shrinkage test was performed. First, the height and weight of the specimens were measured as the initial values. Three parallel specimens were placed on the retractometer, as shown in Figure 5. Then, in a dry state after natural water loss, the mass of the other three specimens was measured once at a designated time each day. The water loss rate was calculated and recorded, and the readings on the dial index of the retractometer were simultaneously recorded. When there was no change in the mean reading over 3 days, the data collection was stopped, and the dry shrinkage test was completed.

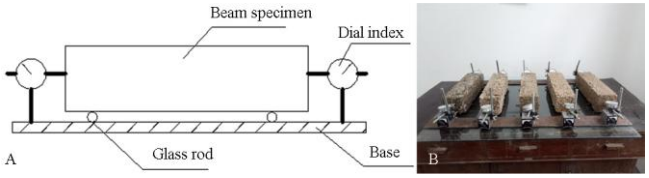

Figure 5. Dry shrinkage test of the beam specimens: a: layout plan; b: test pattern.

$$w_i = (m_i - m_{i+1})/m_p \tag{5}$$

$$\delta_i = \left(\sum_{j=1}^{4} X_{i,j} - \sum_{j=1}^{4} X_{i+1,j} \right) \Big/ 2 \tag{6}$$

$$\varepsilon_i = \delta_i / l \tag{7}$$

$$\alpha_{di} = \varepsilon_i / w_i \tag{8}$$

$$\alpha_d = \sum \varepsilon_i / \sum w_i \tag{9}$$

where w_i is the water loss rate of the *i*th specimen (%) and δ_i is the observed shrinkage amount for the *i*th specimen. First, the values of the two dial indexes at each end were averaged. Then, the mean values (mm) at the two ends were summed. ε_i is the *i*th dry shrinkage strain (%), α_{di} is the *i*th dry shrinkage coefficient (%), m_i is the mass (g) of the standard specimen measured at the *i*th time, $X_{i,j}$ is the *j*th reading (mm) on the dial index for the *i*th testing, *l* is the length (mm) of the standard specimen, and m_p is the mass (g) of the standard specimen after it was dried in a stove.

After the specimens were molded, they were cured to an experimental age of 7 days in a constant-temperature room. Then, the temperature shrinkage test began. The specimens were dried in a high-temperature drying control oven to a constant weight, and their heights were measured. The temperature variation was controlled in the range of 40 ℃ to 0 ℃, as shown in Figure 6. First, the temperature was held at 40 ℃ for 4 hours. The initial readings on the dial index were recorded. Next, the temperature was lowered to 0 ℃, and the specimens were stabilized for another 4 hours. The readings on the dial index were recorded again; these readings were used as the final values. The temperature shrinkage test thus was complete.

The temperature performance parameters were calculated according to Eqs 10 and 11 [25].

$$\varepsilon = (l_b - l_f)/L_0 \tag{10}$$

$$\alpha_t = \varepsilon/(t_b - t_f) \tag{11}$$

where ε is the average shrinkage strain (μm/m) in the temperature variation interval and l_b is the shrinkage amount at the initial stable high temperature (40 ℃). The values on the two dial indexes at each end of the beam specimen were averaged. Then, the mean values (mm) at the two ends were

summed. l_f is the shrinkage amount (mm) at the final stable low temperature (0 ℃), L_0 is the length (mm) of the specimen corresponding to the constant weight of the specimen dried in the oven, α_t is the mean shrinkage coefficient (%/℃) in the temperature variation interval, t_b is the initial stable high temperature (40 ℃), and t_f is the shrinkage amount at the final stable low temperature (0 ℃).

Figure 6. Temperature shrinkage test.

3. Results

3.1. Effects of aggregate gradation on the optimum water content and maximum dry density

The water content-dry density curves of the mixtures of various gradations are shown in Figure 7. Additionally, the maximum dry density and optimum water content are summarized in Table 3, and the variation curves of the maximum dry density and optimum water content are shown in Figure 8.

Table 3. Maximum dry density and optimum water content.

Aggregate gradations	Optimum water content (%)	Maximum dry density (Mg/m^3)
A	4.7	2.380
B	4.8	2.399
C	5.1	2.397
D	5.2	2.389
E	5.4	2.374

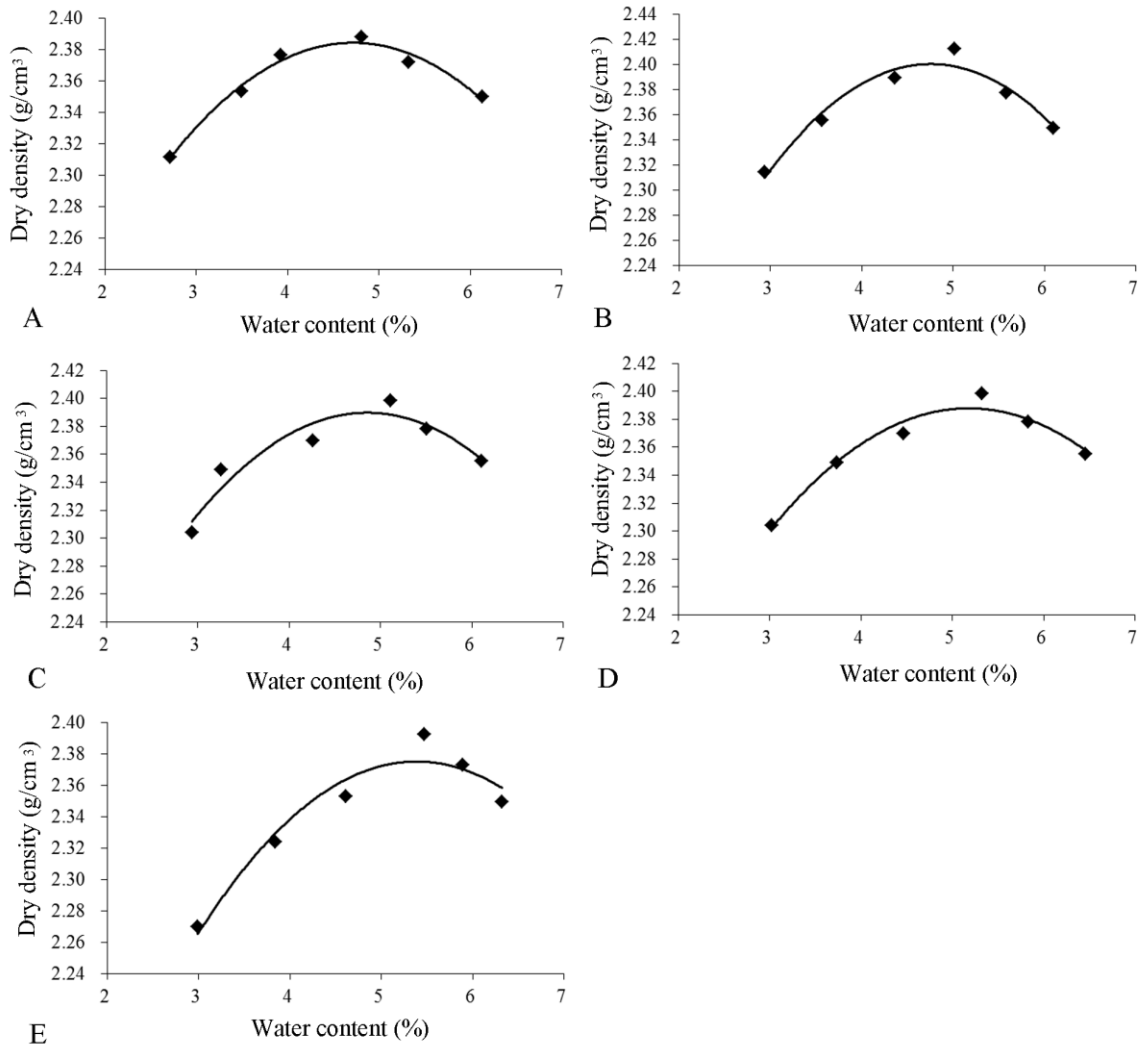

Figure 7. Water content-dry density curves for different gradations: a: Type A; b: Type B; c: Type C; d: Type D; e: Type E.

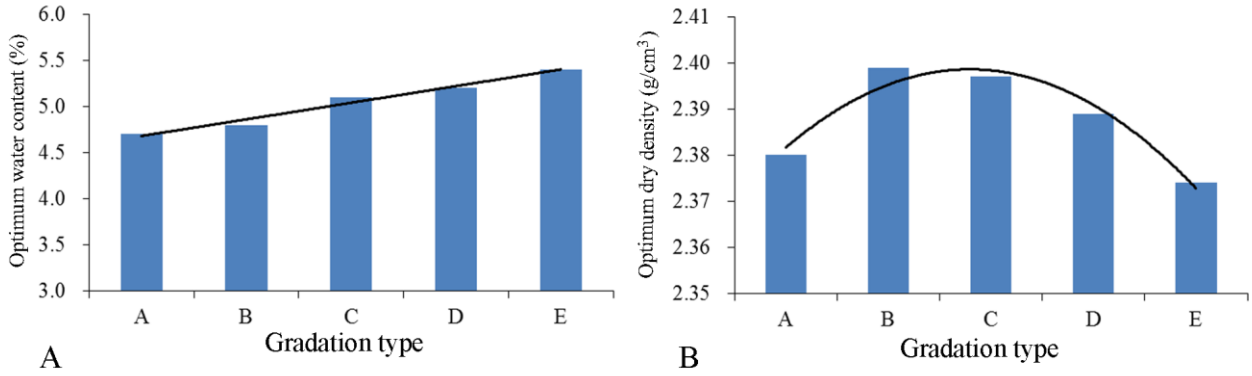

Figure 8. Changes in the optimum water content and optimum dry density according to gradation type: a: optimum water content; b: optimum dry density.

As shown in Figure 8, the optimum water content of CSM tends to increase from Type A to Type E, whereas the maximum dry density tends to initially increase and then decrease. In the gradation range recommended by the current specifications, the gradation variation based on uniform interpolation from A to E represents the overall variation from "coarse-grained" aggregate to "fine-grained" aggregate. A particle size of 4.75 mm is normally regarded as the boundary between coarse-grained and fine-grained aggregates [28,29]. Type A is coarse-grained: its coarse-grained aggregate has a high content (with a sieve-passing rate of 22% at 4.75 mm) and its fine-grained aggregate has a low content. Toward Type E, the aggregate becomes fine-grained: its coarse-grained aggregate has a low content (with a sieve-passing rate of 32% at 4.75 mm) and its fine-grained aggregate has a high content. The trend of the optimum water content in Figure 8A shows that the total surface area of the coarse-grained aggregate is rather small; therefore, less water is adsorbed compared to that observed for the fine-grained aggregate. The incremental variation exhibits a relatively linear trend. If the average passing rate of all particle sizes is regarded as the characteristic variable of the gradation (recorded as P), then the relation between the optimum water content wo and aggregate gradations can be quantified as wo = 0.033 × P + 2.43 (R^2 = 0.98). The optimum water content is closely related to the gradation, which is consistent with the conclusion reported by Liu and Li [20]. However, the results of a previous study suggest that the optimum water content tends to initially decrease and then increase as the aggregate changes from coarse-grained to fine-grained [20]. The optimum water content for the same part of the gradation range displays a decreasing tendency, and the part beyond the gradation range displays an increasing tendency. The main reason for this difference in the results is that the gradation range selected in the previous study was wider than that considered in the current study, and the previous selection method also differs from that used in the current study. In addition, the correlation between the optimum water content and aggregate gradations was not clearly quantified in the previous study [20]. Figure 8B indicates that the maximum dry density of the mixture will peak as the gradation shifts from A to E. The dry density before this peak is mainly affected by the porosity following mixture compaction. The porosity is calculated via Eqs 12 and 13 [26].

$$VCA_{CM} = (a+b)\rho_1 \times 100 / (100+b) / \rho_2 \tag{12}$$

$$VV = VCA_{MIX} - VCA_{CM} \tag{13}$$

where ρ_1 is the maximum dry density (g/cm^3) of the material, ρ_2 is the dry density (g/cm^3) of the cement mortar, VCA_{MIX} is the porosity (%) of the coarse aggregate in the material, VCA_{CM} is the volume ratio (%) of the cement mortar in the material, VV is the material porosity (%), a is the mass percentage (%) of fine aggregate in the gradation, and b is the amount (%) of cement used.

When Type A was used, although it was still within the gradation range of the skeleton dense structure, the content of coarse-grained aggregate was high; therefore, the skeleton porosity VCA_{MIX} was comparatively high. The lower content of fine-grained aggregate could not fill the skeleton voids, leading to a higher total porosity VV (5.8%) for the mixture. Therefore, the dry density was comparatively low. When Type B was adopted, the content of coarse-grained aggregate decreased, the skeleton porosity VCA_{MIX} decreased, and the increased amount of fine aggregate further filled the skeleton voids, leading to a relatively low porosity VV (4.6%). Therefore, the dry density increased.

However, after the peak dry density was reached, the maximum dry density decreased, with the aggregate tending to be finer, mainly due to the apparent density of the aggregate for the given particle sizes. The apparent densities of the aggregates of different particle sizes are shown in Table 4.

Table 4. Apparent density of the aggregates.

Size (mm)	>31.5	19–31.5	9.5–19	4.75–9.5	2.36–4.75	0.6–2.36	0.075–0.6	<0.075
Apparent density (Mg/m^3)	2.720	2.712	2.715	2.682	2.661	2.652	2.650	2.520

Table 4 shows that the apparent densities of the coarse-grained aggregate (above 4.75 mm) are generally higher than those of aggregates with particle sizes below 4.75 mm, which is consistent with the conclusions reported in the literature [30–33]. Therefore, when the gradation changed from Type B to Type E, the content of fine-grained aggregate with a low apparent density increased by 33.3% (from 24.0% for Type B to 32.0% for Type E), whereas the porosity *VV* of the mixture did not exhibit an apparent variation (decreasing from 4.6% for Type B to 4.3% for Type E). However, the maximum dry density continuously decreased. The correlation between the maximum dry density ρmax and aggregate gradations can be quantified as $\rho_{max} = -0.00020 \times P2 + 0.028 \times P + 1.32$ ($R^2 = 0.95$). The above analysis indicates that the maximum dry density is not the median of the range recommended by the specifications; instead, it is less than this value (similar to that of Type B).

3.2. Effect of the aggregate gradation on the mechanical properties

3.2.1. Strength

The test results regarding the CSM strength are summarized in Table 5, and the relations between the CSM strength and gradation type are shown in Figure 9.

Figure 9 shows that when the aggregate gradation changes from Type A to Type E, the unconfined compressive strength of the CSM initially increases rapidly, subsequently increases gradually, and finally decreases. In contrast, the splitting strength exhibits a continuously increasing trend. The strength of the CSM mainly originates from three components: the interlocking effect of the coarse aggregate skeleton, the void effect of the fine aggregate filling the coarse aggregate skeleton, and the cementation effect of the cement and aggregate. The first component plays a major role in the unconfined compressive strength. A better interlocking effect of the skeleton suggests a more dense and stable interlocking between particles and thus a higher unconfined compressive strength of the whole skeleton [5,21]. The splitting strength represents the indirect tensile strength of the material; therefore, the third component plays a dominant role because a stronger cohesiveness of the cement between particles suggests a more favorable tensile strength of the material (stirred uniformity also contributes to the cohesiveness of the cement) [21]. The second component is an auxiliary effect of the unconfined compressive strength and splitting strength. Specifically, better compaction magnifies the other two effects [5,21,22].

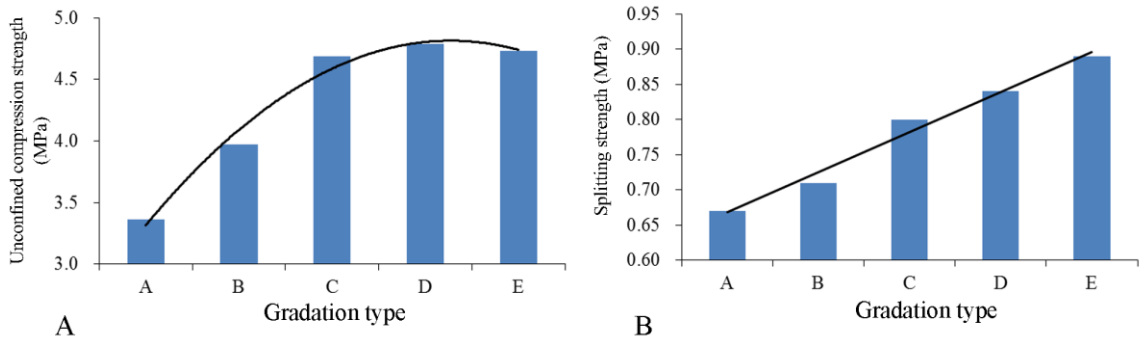

Figure 9. Relations between the CSM strength and gradation type: a: unconfined compressive strength at 7 days; b: splitting strength at 90 days.

Table 5. Material strength.

Aggregate gradations	Compressive strength at 7 days				Splitting strength at 90 days			
	Mean (MPa)	Standard deviation	Variable coefficient (%)	Representative value (MPa)	Mean (MPa)	Standard deviation	Variable coefficient (%)	Representative value (MPa)
A	4.44	0.66	14.78	3.36	0.80	0.08	9.57	0.67
B	4.72	0.46	9.64	3.97	0.77	0.03	4.32	0.71
C	5.43	0.45	8.33	4.69	0.91	0.07	7.85	0.80
D	5.67	0.54	9.46	4.79	0.97	0.08	8.10	0.84
E	5.34	0.37	6.93	4.73	0.94	0.03	2.76	0.89

Representative values are calculated based on a 95% confidence level. Representative value = mean – 1.645 × standard deviation.

Figure 9A indicates that when the coarse gradation Type A is used, the coarse aggregate content is relatively high, and an interlocked skeletal structure is formed. However, the filling effect of the fine aggregate is weak; therefore, the strength is low. When types B and C are adopted, the filling effect of the fine aggregate is considerable as a result of the interlocked skeletal structure. Therefore, the unconfined compressive strength is high (the compressive strength of Type C is nearly 40% higher than that of Type A (Table 5)). However, as the gradation becomes finer, the compressive strength increases, although to a smaller extent, indicating that, at this point, the interlocked skeleton effect is reduced due to further reductions in the coarse aggregate. However, in terms of increasing the compressive strength, the overall effect is weakened (the unconfined compressive strength of Type D is only 3% greater than that of Type C). The compressive strength of Type D is the maximum of all gradations tested, with the unconfined compressive strength of Type E being lower, indicating that the interlocking effect of the coarse aggregate skeleton decreases in magnitude as the gradation becomes finer. Although the fine aggregate filling effect increases in magnitude as the gradation becomes finer, the significance of the effect is relatively small, resulting in a declining unconfined compressive strength of the material. The correlation between the unconfined compressive strength R_c and aggregate gradations can be quantified as $R_c = -0.0046 \times P2 + 0.80 \times P - 30.00$ ($R^2 = 0.98$), and the correlation is high. Figure 9B shows that as the gradation changes from Type A to Type E and the fine aggregate content increases, the porosity of CSM decreases, the compaction increases, and

the cementation effect of the cement and aggregate becomes stronger. Therefore, the splitting strength is continuously enhanced, and the relationship between the splitting strength R_i and aggregate gradation can be quantified as $R_i = 0.010 \times P + 0.045$ ($R^2 = 0.98$), with a good correlation observed. The splitting strength of cement-based materials is directly correlated with their flexural tensile strength [34]; thus, the tendency of the flexural tensile strength index can provide a valuable reference for that of the splitting strength. Liu and Li used skeleton dense gradations (Z, Y, and X) and dense suspension gradations (W, V, and U) to investigate the effect of the aggregate gradation on flexural tensile strength (Figure 10) [20]. They found that the flexural tensile strength increased from gradation Z to gradation X but began to decrease from gradation W (Figure 10). Based on this finding, it is reasonably presumed that if the upper gradation limit in this study is exceeded to form dense suspension gradations [18], the fine aggregate content will continue to increase until the mixture reaches a dense suspension state. However, at this point, material compaction increases, and for a given cement content, the increase in aggregate will lead to an excessive increase in the specific surface area, resulting in a weakening of the cementation effect of the cement and aggregate and a post-peak decrease in the splitting strength.

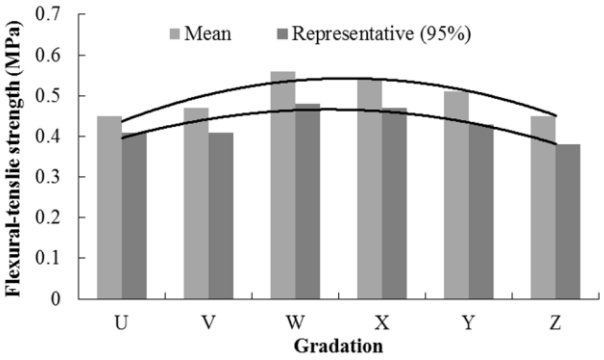

Figure 10. Anti-bending strength of the various gradations at 7 days [20].

3.2.2. Compression rebound modulus

The measurement results of the CSM compression rebound modulus are summarized in Table 6, and the correlation between the CSM compression rebound modulus and gradation is shown in Figure 11.

Table 6. Compression rebound modulus of the material.

Aggregate gradation method	Mean (MPa)	Standard deviation	Variable coefficient (%)	Representative value (MPa)
A	1134	103	9.06	965
B	1173	30	2.59	1123
C	1416	96	6.77	1258
D	1409	75	5.3	1286
E	1232	48	3.87	1153

The representative value is calculated with a 95% confidence level. Representative value = mean – 1.645 × standard deviation.

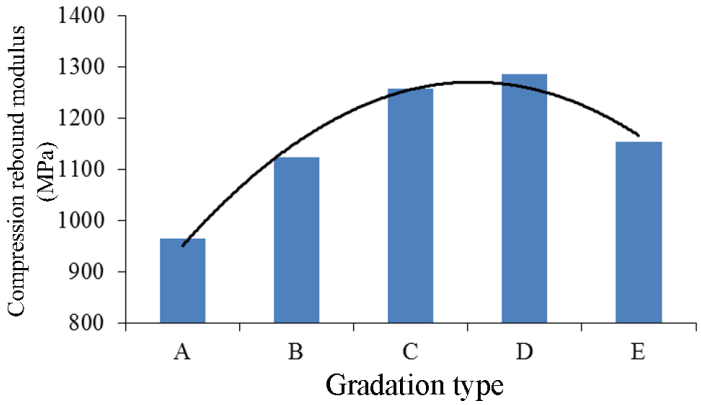

Figure 11. Correlation between the CSM compression rebound modulus and gradation.

Figure 11 shows that the compression rebound modulus of CSM initially increases but subsequently decreases as the aggregate gradation changes from Type A to Type E. The correlation between the compression rebound modulus E_c and aggregate gradations can be quantified as E_c = –1.63 × P2 + 269.72 × P – 9877.90 (R^2 = 0.97), and the basic trend is similar to that of the unconfined compressive strength. The compression rebound modulus and porosity of the CSM material and the skeleton composition state of the aggregate are closely related. As the gradation changes from Type A to Type E, the increase in fine aggregates in the skeleton dense structure causes the material to become more compact and the porosity to decrease, while slightly increasing the compression rebound modulus. Then, as the amount of fine aggregate further increases, the skeleton dense structure is transformed into a suspension structure, and the anti-deformation ability of the material is slightly weakened. Therefore, the compression rebound modulus again exhibits a decreasing trend. The peak value of the compression rebound modulus of CSM is observed for the Type D gradation.

3.3. Effect of the aggregate gradations on the shrinkage performance

The shrinkage test results for the CSM are summarized in Table 7, and the correlation curve between the shrinkage coefficient and the gradations is shown in Figure 12.

Table 7. Material shrinkage coefficient.

Aggregate gradation method	Water loss rate (%)	Dry shrinkage strain (%)	Dry shrinkage coefficient (%)	Temperature shrinkage strain (%)	Temperature shrinkage coefficient (%)
A	2.36	0.00977	0.414	0.0168	0.0000558
B	2.28	0.00768	0.337	0.0187	0.0000623
C	2.60	0.01058	0.407	0.0235	0.0000784
D	2.75	0.01770	0.644	0.0266	0.0000885
E	2.82	0.03345	1.185	0.0345	0.0000115

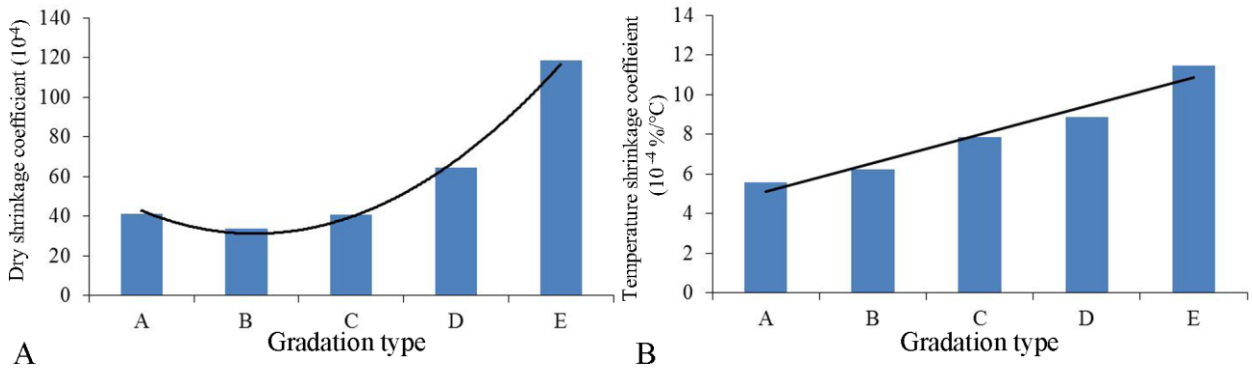

Figure 12. Correlation between the shrinkage coefficient and gradations: a: dry shrinkage coefficient (10^{-4}); b: temperature shrinkage coefficient (10^{-4} %/ ℃).

Figure 12 shows that the shrinkage coefficient gradually increases as the gradation changes from Type A to Type E. However, the dry shrinkage coefficient rapidly increases (the dry shrinkage coefficient of Type E nearly doubles compared to that of Type A). The correlation between the dry shrinkage coefficient and the gradations can be captured by the quadratic curve $a_d = 0.33 \times P2 - 49.65 \times P + 1882.70$ ($R^2 = 0.99$) and exhibits an increasing trend with a good correlation. The temperature shrinkage coefficient steadily increases and exhibits a linearly increasing trend with a high correlation: $a_t = 0.26 \times P - 12.93$ ($R^2 = 0.95$).

Dry shrinkage is mainly caused by the material water loss and carbonization common to cement-based materials [35,36]. These processes both occur prior to the closure of the base structure and are concurrent. Additionally, they lead to the dry shrinkage and cracking of CSM, especially under heavy traffic conditions. Figure 8A shows that the optimum water content of the fine-grained aggregate is higher than that of the coarse-grained aggregate. The water loss rate of the fine-grained CSM is also high; therefore, the dry shrinkage coefficient gradually increases as the gradation changes from coarse to fine. Temperature shrinkage is caused by changes in temperature. Figure 12B shows that a finer gradation (i.e., a high proportion of fine aggregate) causes the CSM to be more prone to temperature shrinkage deformation, which also confirms the main principles and requirements in classifying the CSM structure type reported by the Ministry of Communications of PRC [18].

4. Conclusion

In this study, five gradations (A–E) were obtained by the uniform interpolation method based on the skeleton dense structure CSM and aggregate gradation range recommended by the current specifications. The main findings were as follows.

(1) Aggregate gradation has a noticeable influence on the performance of CSM roads, and the relation between them can be quantified.

(2) As the aggregate gradation shifts from Type A to Type E, the optimum water content, splitting strength, dry shrinkage coefficient and temperature shrinkage coefficient of the CSM increase, whereas the maximum dry density, compressive strength and compression rebound modulus show an increase followed by a gradual decrease.

(3) With the increase in the proportion of fine aggregate as the gradation shifts from Type A to Type E, the anti-temperature shrinkage deformation ability of the CSM is gradually weakened. The maximum density is not the median of the range recommended by the current specifications (that of gradation C) but instead occurs below the median value (similar to that of gradation B).

Compared with the current literature, this study conducted a comprehensive investigation of the correlation between gradation type and the associated performance parameters. Furthermore, the parameters in this study were relatively inclusive. In actual engineering, the optimum gradation cannot be achieved in most cases. The correlations obtained in this study can be used to assess the CSM performance parameters used for actual gradation. In addition, the optimum values of the unconfined compressive strength and compression rebound modulus of CSM were observed for the Type D gradation. If the shrinkage coefficient of the material is decreased, a low fine aggregate content is preferred. The aggregate gradation design in actual engineering should be based on the specific requirements for CSM performance.

This study was conducted based on CSM with a skeleton dense structure and thus failed to cover other gradation types, i.e., skeleton void structure and skeleton suspension structure. To improve the completeness of the current findings, studies on these gradation types remain to be carried out in the future.

Acknowledgments

This study was supported by the academic frontier special scientific research project of China University of Mining and Technology (Grant No. 2017XKQY050).

Conflict of interest

The authors declare no conflicts of interest in this paper.

References

1. C. Berthelot, D. Podborochynski, B. Marjerison, et al., Mechanistic characterization of cement stabilized marginal granular base materials for road construction, *Can. J. Civil Eng.*, **37** (2010), 1613–1620.
2. J. P. Bilodeau, C. O. Plamondon and D. Guy, Estimation of resilient modulus of unbound granular materials used as pavement base: combined effect of grain-size distribution and aggregate source frictional properties, *Mater. Struct.*, **49** (2016), 4363–4373.
3. Z. J. Chen, J. S. Xue, F. Cao, et al. Study of strong interlocked skeleton dense gradation for cement-stabilized macadam, *Appl. Mech. Mater.*, **438–439** (2013), 644–648.
4. W. S. Guthrie, M. S. Shea and D. L. Eggett, Hydraulic conductivity of cement-treated soils and aggregates after freezing, *Proc. Int. Conf. Cold Reg. Eng.*, **2012** (2012), 93–103.
5. Y. Wang, X. Ma and Z. L. Sun, Shrinkage performance of cement-treated macadam base materials, *ICTTS*, **383** (2010), 1378–1386.
6. W. B. Ashraf and M. A. Noor, Performance-evaluation of concrete properties for different combined aggregate gradation approaches, *Proc. Eng.* **14** (2011), 2627–2634.

7. K. A. Davis, L. S. Warr, S. E. Burns, et al., Physical and chemical behavior of four cement-treated aggregates, *J. Mat. Civil Eng.,* **19** (2007), 891–897.
8. Z. J. Liu, Experimental research on the engineering characteristics of polyester fiber-reinforced cement-stabilized macadam, *J. Mat. Civil Eng.,* **27** (2015), 04015004.
9. Z. J. Liu, Influence of rainfall characteristics on the infiltration moisture field of high-way subgrade, *Road Mat. Pavement.,* **16** (2015), 635–652.
10. I. D. Rey, J. Ayuso, A. Barbudo, et al., Feasibility study of cement-treated 0–8 mm recycled aggregates from construction and demolition waste as road base layer, *Road Mat. Pavement.,* **17** (2016), 678–692.
11. F. Colangelo and R. Cioffi, Mechanical properties and durability of mortar containing fine fraction of demolition wastes produced by selective demolition in South Italy, *Composite B Eng.,* **115** (2017), 43–50.
12. F. Colangelo, R. Cioffi, B. Liguori, et al., Recycled polyolefins waste as aggregates for lightweight concrete, *Composite B Eng.,* **106** (2016), 234–241.
13. V. Corinaldesi, Mechanical and elastic behaviour of concretes made of recycled-concrete coarse aggregates, *Constr. Build. Mat.,* **24** (2010), 1616–1620.
14. W. B. Ashraf and M. A. Noor, Performance-evaluation of concrete properties for different combined aggregate gradation approaches, *Proc. Eng.,* **14** (2011), 2627–2634.
15. M. R. Fatmi, B. Islam, M. Rahman, et al., Optimized aggregate gradation for Bangladesh, *Appl. Mech. Mat.,* **71–78** (2011), 4226–4229.
16. L. Jin and J. L. Zheng, The analysis about how gradation impact on the performance of cement stabilized macadam base, In: 2012 International Conference on Computer Distributed Control and Intelligent Environmental monitoring, Hunan, China, 2012.
17. M. D. Cook, A. Ghaeezadah, and M. T. Ley, Impacts of coarse-aggregate gradation on the workability of slip-formed concrete, *J. Mat. Civil Eng.,* 2018.
18. The Ministry of Communications of PRC. Technical guidelines for construction of highway roadbases (JTG/T F20-2015). China Communication Press, Beijing, China, 2015.
19. G. H. Hu, Study on the influence of the cement stabilized macadam's gradation to the modulus and strength, *Adv. Mat. Res.,* **1004–1005** (2014), 1579–1584.
20. J. X. Liu and B. Li, Optimum design of aggregate gradation for cement stabilized macadam based on the fuzzy orthogonal method, *J. Wuhan Univ. Tech.,* **32** (2010), 60–64.
21. Y. Wang, F. J. Ni and W. H. Xuan, Research on dry shrinkage performance of cement-treated base materials, *Geohunan Int. Conf.,* **2009** (2009), 81–86.
22. Y. Wang, X. Sun, and Z. X. Li, Research on the reasonable strength of cement-treated macadam base, *Adv. Civil Eng. Build. Mat.,* **2012** (2012), 621–624.
23. Y. Wang, W. H. Xuan and X. T. Feng, Studies on fatigue behaviors of cement stabilized macadam mixture, *Geohunan Int Conf.,* 2011. Available from https://ascelibrary.org/doi/pdf/10.1061/47629(408)14.
24. Y. J. Jiang, L. W. Li, Y. S. Xu, et al. Performance comparison of cement-stabilized macadam with two skeleton close-grained gradation, *Int. Conf. Concrete Pavement Des. Constr. Rehabil.,* **2011** (2011), 71–75.
25. The Ministry of Communications of PRC. Test methods of materials stabilized with inorganic binders for highway engineering (JTG E51-2009). China Communication Press, Beijing, China, 2009.

26. P. Zhang, Q. F. Li and H. Wei, Investigation of flexural properties of cement-stabilized macadam reinforced with polypropylene fiber, *J. Mater. Civil Eng.,* **22** (2010), 1282–1287.
27. L. J. Zhao, W. Z. Jiang, J. R. Hou, et al., Influence of mixing methods on performance of compressive strength for cement stabilized macadam mixture, *China J. Highway Transport.,* **31** (2018), 151–158.
28. Y. B. Yang, H. M. Chen and S. M. Wu, Study on the C80 high-strength rock chips concrete, Key Engineering Materials, *Ecol. Environ. Tech. Concrete,* **477** (2011), 218–223.
29. Y. L. Zhao, Gradation design of the aggregate skeleton in asphalt mixture, *J. Test. Eval.,* **40** (2012), 20120142.
30. L. H. Li, P. Huang and D. Liu, Impact on performance of cement stabilized macadam mixtures between gyratory compaction and static compaction methods, *J. Chang'an Univ. (Nat. Sci. Ed.),* **36** (2016), 17–25.
31. D. Luo and C. F. Wu, Influence of gradation and compaction standards to performance of cement stabilized crushed stone base material, *Highway,* **4** (2014), 187–193.
32. T. Ma, X. H. Ding, D. Y. Zhang, et al., Experimental study of recycled asphalt concrete modified by high-modulus agent, *Constr. Build Mat.,* **128** (2016), 128–135.
33. X. Yu and X. Wu, The influences of RAP on the performance of cement stabilized crushed stone base, *IEEE,* **2011** (2011), 6315–6318.
34. M. O. Ahmed, A. H. Waddah and K. Manish, Research on the mechanical strength of emulsified asphalt-cement stabilized macadam based on neural network algorithm, *Key Eng. Mat.,* **753** (2017), 326–330.
35. A. Muntean, M. Böhm and J. Kropp, Moving carbonation fronts in concrete: A moving-sharp-interface approach, *Chem. Eng. Sci.,* **66** (2011), 538–547.
36. I. S. Yoon, O. Çopuroğlu and K. B. Park, Effect of global climatic change on carbonation progress of concrete, *Atmos. Environ.,* **41** (2007), 7274–7285.